CdS_xSe_{1-x}/ZnS semiconductor nanocrystal laser with sub 10kW/cm^2 threshold and 40nJ emission output at 600 nm

Luke Jonathan McLellan, Benoit Guilhabert, Nicolas Laurand and Martin D. Dawson

Institute of Photonics, Department of Physics, University of Strathlcyde, Glasgow, G1 1RD, UK
*luke.mclellan@strath.ac.uk

Abstract: A colloidal quantum dot laser emitting at 600 nm with a sub 10kW/cm^2 threshold at 5ns pulse pumping is reported. The device has a second order distributed feedback cavity for vertical emission and incorporates a bilayer planar waveguide structure based on a film of yellow-orange alloyed-core/shell CdS_xSe_{1-x}/ZnS quantum dots over-coated with polyvinyl alcohol. A study of the amplified spontaneous regime indicates that the quantum dot gain region behaves like a quasi-three level system and that the bilayer structure design increases the modal gain compared to a single layer of quantum dots. An output of 40nJ per pulse is measured for a total pump-to-signal efficiency above threshold of 3%.

OCIS codes: (000.0000) General; (000.2700) General science.

References and links

1. J. Y. Kim,O. Voznyy, D. Zhitomirsky, & E.H. Sargent, "25th Anniversary Article: Colloidal Quantum Dot Materials and Devices: A Quarter-Century of Advances." Advanced Materials, **25**, 4986–5010 (2013).
2. P. Reiss, M. Protière & L. Li, "Core/Shell semiconductor nanocrystals." Small (Weinheim an Der Bergstrasse, Germany), **5**(2), 154–68 (2009).
3. F. Todescato, I. Fortunati, S. Gardin, E. Garbin, E. Collini, R. Bozio, J. J. Jasieniak, G. Della Giustina, G. Brusatin, &R. Signorini, "Soft-Lithographed Up-Converted Distributed Feedback Visible Lasers Based on CdSe-CdZnS-ZnS Quantum Dots." Advanced Functional Materials, **22**(2), 337–344 (2012).
4. V. C.Sundar, H. J. Eisler, T. Deng, Y. Chan, E. L. Thomas, & M.G. Bawendi, "Soft-Lithographically Embossed, Multilayered Distributed-Feedback Nanocrystal Lasers." Advanced Materials, **16**(23-24), 2137–2141 (2004).
5. B. Guilhabert, C. Foucher, A. Haughey, E. Mutlugun, J. Herrnsdorf, H. D. Sun, H. V. Demir, & M. D. Dawson, "Nanosecond colloidal quantum dot lasers for sensing". Optics Express, **22**(6), 602–606 (2014).
6. Q. Sun, Y. Wang, L. S. Li, D. Wang, T. Zhu, J. Xu, C. Yang, & Y. Li, "Bright, multicoloured light-emitting diodes based on quantum dots," Nature Photon. **1**, 717–722 (2007).
7. T. H. Kim, K. S. Cho, E. K. Lee, S. J. Lee, J. Chae, J.W. Kim, D. H. Kim, J. Y. Kwon, G. Amaratunga, S. Y. Lee, B. L. Choi, Y. Kuk, J. M. Kim, & K. Kim, "Full-colour quantum dot displays fabricated by transfer printing," Nature Photon. **5**, 176–182 (2011).
8. P. Spinicelli, B. Mahler, S. Buil, X. Quélin, B. Dubertret & J.P. Hermier, "Non-blinking semiconductor colloidal quantum dots for biology, optoelectronics and quantum optics." ChemPhysChem, **10**(6), 879–882 (2009).
9. V. Bagalkot, L. Zhang, E. Levy-Nissenbaum, S. Jon, P. W. Kantoff, R. Langer, & O. C. Farokhzad, "Quantum dot-aptamer conjugates for synchronous cancer imaging, therapy, and sensing of drug delivery based on bi-fluorescence resonance energy transfer." Nano Letters, **7**(10), 3065–70 (2007).
10. J. Shi, C. Chan, Y. Pang, W. Ye, F. Tian, J. Lyu, Y. Zhang, & M. Yang. "A fluorescence resonance energy transfer (FRET) biosensor based on graphene quantum dots (GQDs) and gold nanoparticles (AuNPs) for the detection of mecA gene sequence of Staphylococcus aureus." Biosensors and Bioelectronics, **67**, 595–600. (2015).

11. X. Gao, L. Yang, J.a. Petros,F. F. Marshall, J. W. Simons, & S. Nie, “In vivo molecular and cellular imaging with quantum dots.” Current Opinion in Biotechnology, **16**(1), 63–72 (2005).
12. S. Nizamoglu, G. Zengin & H. V. Demir, “Color-converting combinations of nanocrystal emitters for warm-white light generation with high color rendering index.” Applied Physics Letters, **92**(3), 031102 (2008).
13. S. Chanyawadee, P. G. Lagoudakis, R. T. Harley, M. D. B. Charlton, D. V. Talapin, H. W. Huang, & C. H. Lin, “Increased color-conversion efficiency in hybrid light-emitting diodes utilizing non-radiative energy transfer.” Advanced Materials (Deerfield Beach, Fla.), **22**(5), 602–6 (2010).
14. E. Mutlugun, P. L. Hernandez-Martinez, C. Eroglu, Y. Coskun, T. Erdem, V. K. Sharma & H. V. Demir, “Large-area (over 50 cm × 50 cm) freestanding films of colloidal InP/ZnS quantum dots.” Nano Letters, **12**(8), 3986–93 (2012).
15. B. Guzelturk, Y. Kelestemur, K. Gungor, A. Yeltik, M. Z. Akgul, Y. Wang, C. Rui, D. Cuong, S. Handong, & H. V. Demir. “Stable and Low-Threshold Optical Gain in CdSe/CdS Quantum Dots: An All-Colloidal Frequency Up-Converted Laser.” Advanced Materials, **27**(17), 2741–2746. (2015).
16. S. Kim, R. Sharma, B. Kim, H. S. Yang & K. Kyhm, “Modal gain enhancement by cylindrical waveguide and gain saturation in CdSe nanocrystal quantum dots.” Journal of Physics D: Applied Physics, **42**(9), 095403. (2009).
17. V. I. Klimov, A. A. Mikhailovsky, Su Xu, A. Malko, J. A. Hollingsworth, C. A. Leatherdale, H.-J. Eisler, & M. G. Bawendi, “Optical Gain and Stimulated Emission in Nanocrystal Quantum Dots”. Science, **290**(5490), 314–317 (2000).
18. M. a. Hines & P. Guyot-Sionnest, “Synthesis and Characterization of Strongly Luminescing ZnS-Capped CdSe Nanocrystals.” The Journal of Physical Chemistry, **100**(2), 468–471 (1996).
19. A. F. Cihan, Y. Kelestemur, B. Guzelturk, O. Yerli, U. Kurum, H.G. Yaglioglu, A. Elmali, & H. V. Demir. “Attractive versus Repulsive Excitonic Interactions of Colloidal Quantum Dots Control Blue- to Red-Shifting (and Non-shifting) Amplified Spontaneous Emission.” Journal of Physical Chemistry Letters, **4**(23). (2013).
20. Y. Chen, B. Guilhabert, J. Herrnsdorf, Y. Zhang, A. R. Mackintosh, R. A. Pethrick, E. Gu, N. Laurand, & M. D. Dawson, “Flexible distributed-feedback colloidal quantum dot laser.” Applied Physics Letters, **99**(24), 241103 (2011).
21. Dang & A. Nurmikko, “Beyond quantum dot LEDs: Optical gain and laser action in red, green, and blue colors.” MRS Bulletin, **38**(09), 737–742 (2013).
22. Foucher, B. Guilhabert, N. Laurand, & M. D. Dawson. “Wavelength-tunable colloidal quantum dot laser on ultra-thin flexible glass”. Applied Physics Letters, **104**(14), 141108. (2014).
23. A. Y. Wang, K. S. Leck, V. D. Ta, R. Chen, V. Nalla, Y. Gao,T. He, H. V. Demir, & Sun, H. “Blue Liquid Lasers from Solution of CdZnS/ZnS Ternary Alloy Quantum Dots with Quasi-Continuous Pumping.” Advanced Materials, **27**(1), 169–175. (2014).
24. Y. Wang, K. E. Fong, S. Yang, V. D. Ta, Y. Gao, Z. Wang, V. Venkatram, H. V. Demir,& H. Sun. “Unraveling the ultralow threshold stimulated emission from CdZnS/ZnS quantum dot and enabling high-Q microlasers.” Laser & Photonics Reviews, **9**(5), 507–516. . (2015).
25. G. E. Cragg & A. L. Efros, “Suppression of auger processes in confined structures.” Nano Letters, **10**(1), 313–7 (2010).
26. Y. S. Park, W. K. Bae, J. M. Pietryga, & Klimov, V. I. “Auger recombination of biexcitons and negative and positive trions in individual quantum dots.” ACS Nano, **8**(7), 7288–7296. (2014).
27. Y. Park, W. K. Bae, L. A. Padilha, M. Pietryga, & V. I. Klimov. “Effect of the Core/Shell Interface on Auger Recombination Evaluated by Single-Quantum-Dot Spectroscopy.” Nano Letters, **14**(2), 396–402. (2014).
28. Y-S. Park, W. K. Bae, T. Baker, J. Lim, & V.I. Klimov. “Effect of Auger Recombination on Lasing in Heterostructured Quantum Dots with Engineered Core/Shell Interfaces.” Nano Letters, **15**(11), 7319–7328. (2015).
29. C. Foucher, B. Guilhabert, a. L. Kanibolotsky, P. J. Skabara, N. Laurand, & M. D. Dawson “Highly-photostable and mechanically flexible all-organic semiconductor lasers.” Optical Materials Express, **3**(5), 584 (2013).
30. R. E. Bailey & S. Nie, “Alloyed semiconductor quantum dots: tuning the optical properties without changing the particle size.” Journal of the American Chemical Society, **125**(23), 7100–6 (2003).

31. T. Liptay, L. Marshall, P. Rao, R. Ram & M. G. Bawendi, "Anomalous Stokes shift in CdSe nanocrystals." Physical Review B, **76**(15), 155314. (2007).
32. Joshi, K. Y. Narsingi, M. O. Manasreh, E. a. Davis & B. D. Weaver "Temperature dependence of the band gap of colloidal CdSe/ZnS core/shell nanocrystals embedded into an ultraviolet curable resin." Applied Physics Letters, **89**(13), 89–92 (2006).
33. O. Svelto, "Principles of Lasers", (1974).
34. Y. Chen, J. Herrnsdorf, B. Guilhabert, Y. Zhang, I.M. Watson, E. Gu, N. Laurand & M. D. Dawson. "Colloidal quantum dot random laser." Optics Express, **19**(4), 2996–3003(2011).
35. O. Svelto, S. Taccheo, & C. Svelto. Analysis of amplified spontaneous emission: some corrections to the Linford formula. Optics Communications, 149(4-6), 277–282. (1998).
36. V. Navarro-Fuster, I. Vragovic, E. M. Calzado, P.G. Boj, J. a. Quintana, J. M. Villalvilla, A. Retolaza, A. Juarros, D. Otaduy, S. Merino, & M. A. Díaz-García. "Film thickness and grating depth variation in organic second-order distributed feedback lasers." Journal of Applied Physics, **112**(4), 043104. (2012).

1. Introduction

Colloidal quantum dots (CQDs) are semiconductor nanocrystals (size < 10 nm) that confine carriers in three dimensions and are inherently compatible with solution processing [1]. By adjusting their mean size and/or their semiconductor composition, they can be made to emit light efficiently across a wide range of wavelengths [2]. They can be combined with both organic and inorganic materials to form composites and, e.g., can be patterned by soft lithography [3,4]. In turn, CQDs are finding applications in biological imaging, optoelectronics [5-14] and have also great potential as a laser material [15-24]. This is especially the case for visible lasers where the quantisation of the density of states in II-VI CQDs coupled with the flexibility of solution processing holds the promise for innovative formats of lasers at wavelengths that are important for applications but difficult to access with other laser materials, e.g. in the yellow-orange part of the spectrum [2,16-20]. However, despite much attention and developments in the last 15 years, CQD lasers are not yet practical sources. For this, optical pumping with nanosecond or longer pulses is necessary for the technology to be compatible with compact solid-state pump lasers [21, 22] and, ultimately, with laser diodes.

The aim of this work is to push the performance of CQD lasers when operated in such a temporal regime. A distributed feedback laser (DFB) with a bilayer planar waveguide structure is reported where the gain region consists of alloyed-core/shell CdS_xSe_{1-x}/ZnS CQDs. The bilayer waveguide structure enhances the modal gain while an alloyed-core/shell CQD design is known to help mitigate the issue of Auger recombination, which can be significant in CdSe/ZnS [17, 25-28].

In the following, section 2 describes in details the design and fabrication of the DFB laser cavity. Section 3 summarises the experimental methods and arrangements of the different characterisation set-ups. Section 4.1 reports on the photoluminescence (PL) and amplified spontaneous emission (ASE) characteristics of the equivalent planar waveguide, independently of the DFB cavity. In this section, it is shown that the CdS_xSe_{1-x}/ZnS CQDs behaves like a quasi-3-level laser medium. Finally, section 4.2 demonstrates laser emission at 600 nm with threshold below 10 kW/cm^2.

2. Design and fabrication of the laser

The design of the laser is shown in Fig. 1(a). It is based on a DFB cavity with a bi-layer, planar waveguiding structure. The first of these layers is a 300nm thick CQD film (the gain layer) that sits on top of a surface-patterned glass substrate. The second layer, over-coating the CQD film, is made of polyvinyl alcohol (PVA). The PVA has two roles: (i) it acts as an encapsulating barrier for oxygen [29] and (ii) it symmetrises the refractive index profile of the laser structure. The latter improves the confinement of the laser mode inside the planar guide structure, helping reducing the effect of surface scattering losses and hence increasing the modal gain, which is critical for low threshold performance. The thickness of the PVA layer

was chosen to be 180 nm as a trade-off between confinement, overlap of the mode with the CQD layer and barrier properties [29].

The period of the rectangular nanopattern, the DFB grating, on the surface of the fused silica glass substrate (refractive index of 1.46), is Λ=380 nm and the the modulation depth of this pattern is 50 nm. The period is chosen to obtain a 2nd order DFB effect with optical feedback for the laser mode happening via the second order of diffraction and vertical emission (from the top and bottom of the laser structure) through the 1st order of diffraction, Fig. 1(a). The mask for the nanopattern was defined by e-beam lithography and its transfer into the glass substrate was done by dry etching.

The CdS_xSe_{1-x}/ZnS CQDs are Trilite™ from Cytodiagnostics with an intrinsic PL centred at 575 nm. These are type I alloyed-core/shell structures with an average size of 6 nm and oleic acid as surface ligands. Auger recombination is known to be a limiting factor for laser performance in spherical type I CQDs, which is enhanced by the abrupt core/shell interface, and this detrimental effect is intensified in CQDs of smaller size [25]. An alloyed-core design [30] enables the use of CQDs with a relatively large size over a range of emission wavelengths (e.g. 6nm diameter for emission from 450 nm to 665 nm for Trilite™ CQDs) while possibly smoothing the abrupt core/shell energy interface. The 575nm CQDs used for this work were initially in toluene at a concentration of 1 $mg.mL^{-1}$. Fig. 1(b) shows the absorption, overlaid with the photoluminescence (PL) spectra, in solution, of the CQDs (see section 3 for details on measurements). The first absorption peak occurs at 557 nm and the Stokes shift is 21 nm. The magnitude of the Stokes shift is similar to that of typical core/shell CdSe/ZnS CQDs [31,32]. Generally, a high Stokes shift is desirable for CQD lasers as it minimizes re-absorption effect in the gain material.

For fabrication, the toluene was evaporated using a vacuum pump in order to obtain the CQDs in powder form. The CQDs were then re-diluted at 50 $mg.mL^{-1}$ in a Poly (methyl methacrylate) (PMMA): chloroform mix with a weight ratio PMMA to chloroform 1.6:1. The solution was spun cast onto the glass substrate at 4krpm for 60 seconds. After deposition of the PVA (prepared as in [29]), also by spin-coating at 3.2krpm for 60 seconds, the sample was annealed at 30ºC for 120 hours.

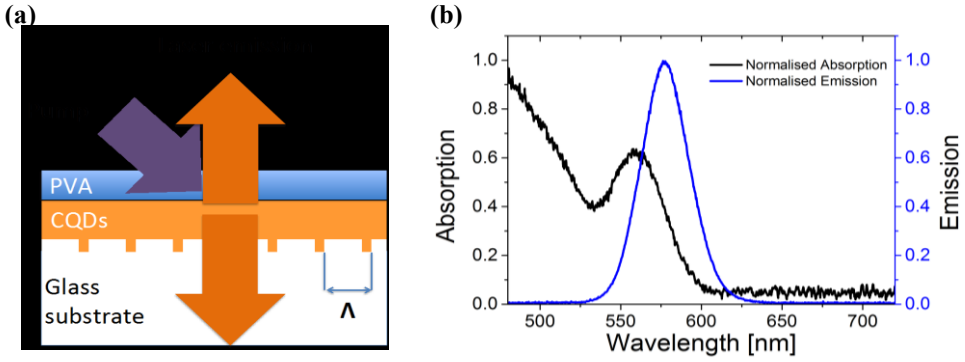

Fig. 1:(a) Schematic of the laser structure with grating substrate, Λ = 380nm, 300nm CQD layer and 180nm PVA layer. The laser is pumped at an angle (blue/puple arrow) and has vertical emission (orange arrows) (b) absorption and emission spectra of 575nm.

3. Experimental Methods

For the absorption and PL measurements in solution shown in Fig. 1(b), a small amount of CdS_xSe_{1-x}/ZnS CQDs at $1mg.mL^{-1}$ in toluene was placed into a 1mm-path glass cuvette. For PL in solution, a 10mW UV laser diode emitting at 371 nm was used as the pump source and

the spectrum was recorded with a TRIAX 550 spectrometer at a resolution of 0.03 nm. For absorption measurements, the pump source was a tungsten lamp. The light transmitted through the cuvette was collected for recording the spectrum using the aforementioned spectrometer. Measurements were calibrated with respect to the transmission data taken through the cuvette filled only with toluene.

The PL and ASE characteristics of the bilayer CQD gain film/PVA structure discussed in section 4.1 were measured independently of the DFB laser cavity by forming the equivalent waveguide structure onto smooth glass, i.e. same as the laser structure but with no DFB grating – such structure is called 'CQD/PVA sample' in the following. To verify the effect of the PVA layer, the ASE performance of a CQD film on glass with no PVA overcoating was also characterised – this structure is called 'CQD sample'. The continuous-wave (cw) edge PL emission measurements of the CQD films were done using the 371nm laser diode as the pump with a beam shaped as a 6.1±0.4 mm by 1.7±0.2 mm stripe onto the film surface. The emission from the edge of the film was then collected with a microscope objective (60 X magnification, NA 0.85) where the spectrum was measured using the same TRIAX spectrometer as previously. For the detection of ASE the CQD and the CQD/PVA samples were pumped with 5ns-pulses from a Nd:YAG laser emitting at 355 nm at a repetition rate of 10 Hz. The pump beam in this case was a stripe of 8.3 mm by 1.0 mm positioned near the edge of the film surface and the emission was directly collected from the edge of the sample by a 50μm-core optical fibre placed at 0.5 cm. The latter was connected to a CCD spectrometer (Avantes, 2.5nm resolution); the spectrum for different level of pump energy was recorded.

The same Nd:YAG pump laser source was also utilised for the demonstration and characterisation of the DFB lasers (section 4.2) with an excitation area of 0.74±0.01 mm by 4.4±0.2 mm. The vertically emitted laser emission from the device (devices were sitting at a slight angle with respect to the pump), was collected for analysis. Spectral measurements were done using a fibre-coupled CCD spectrometer with a 0.13nm resolution

4. Results and Discussion

4.1 Study of ASE

Fig. 2 represents the edge PL peak intensity as a function of the pump fluence for, respectively, the CQD sample and the CQD/PVA sample. The inset shows the spectrum of the CQD/PVA sample at different fluence. Both intensity curves follow a similar trend: at lower fluence, the intensity increase with the fluence is sublinear before becoming supralinear above a certain pump level (where the transitions from PL to ASE occur at F_{ASE}>800 μJ/cm^2 for the CQD sample and F_{ASE} > 380 μJ/cm^2 for the CQD/PVA). In both cases, the edge emission is made of two contributions: (i) an unamplififed component of the PL, that couples into the detection fibre and (ii) an amplified component of the PL made of photons that are confined along the excitation stripe. The unamplified PL is predominant at low fluence and the sublinear behaviour can be explained partly by an increase of the pumping transverse efficiency with the fluence [33]. Because of the Gaussian profile of the pump intensity and its depletion as it is absorbed in the transvere direction (along the thickness of the film) at lower fluence only the gain region near the beam axis and the top of the of the CQD film contributes to stimulated emission while other parts of the gain region give off only spontaneous emission. As fluence increases, a larger fraction of the excited volume reaches the regime of optical gain, in turn increasing and reducing, respectively, stimulated and spontaneous

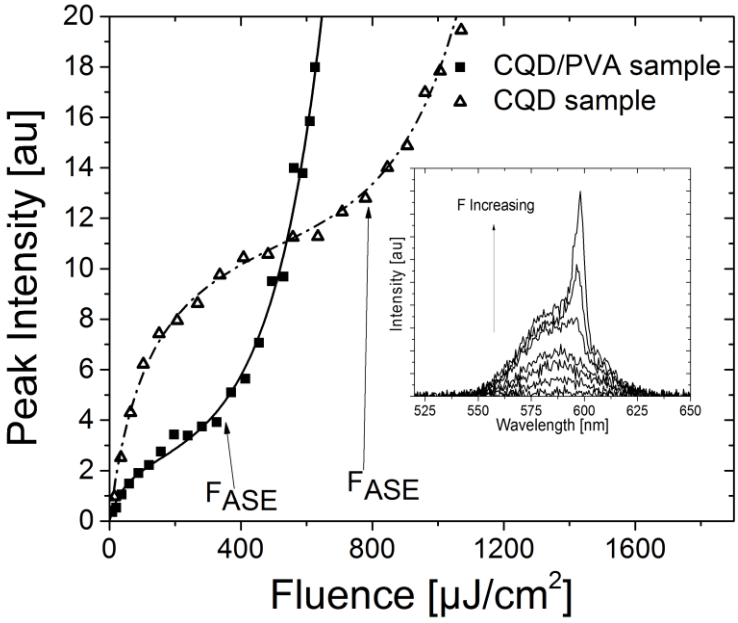

Fig. 2: Edge PL peak intensity versus pump fluence for the CQD sample (data - open triangle; fit – dash-dot line) and CQD/PVA sample (data – black squares; fit – solid black line). Insert: Typical spectrum evolution (for increasing pump energy.

emission. The saturation of the 1S excitonic level could also play a role in the reduction of the slope of detected PL and a similar behavior was previously seen in films of CdSe/ZnS CQDs [34]. The amplified component fully dominates at the higher fluence regime when all spontaneously emitted photons that are guided in the CQD layer are amplified significantly by stimulated emission. In this ASE regime the intensity increase with fluence is exponential as long as gain saturation is not reached while the spectrum transitions from a broad PL peak to a narrower ASE peak (see inset of Fig. 2 and Fig. 3). The onset of ASE appears at a lower fluence for the CQD/PVA sample, as can be seen in Fig. 2, due to the added PVA layer reducing the mode intensity at the laser surface, enabling a higher net optical gain to be extracted.

The data of Fig. 2 is fitted by considering the two aforementioned contributions to the edge emission, as displayed in Fig. 2 as a dash-dot line for the CQD sample and a solid line for the CQD/PVA sample. The intensity evolution in the ASE regime is approximated as [35]:

$$\mathrm{I_{edge}} = \mathrm{I_{ASE}} + \mathrm{I_{naPL}} = \mathrm{A}\frac{(\mathrm{G}-1)^{3/2}}{(\mathrm{Gln(G)})^{1/2}} + \mathrm{I_{naPL}} \qquad (1)$$

In (1) A is a fit parameter and G is the single-pass gain given by $G = \exp(gL)$ where g is the net modal gain, L is the effective amplifier length and the product gL is taken as $gL = B \cdot F$. B is proportional to the gain factor of the CQD layer and F is the pump fluence. I_{edge} is the peak intensity collected at the edge of the sample. The term I_{naPL} is considered phenomenologically as a saturating phenomenon. It is determined by fitting the data at the lowest fluence only where I_{ASE} is neglected. This then enables fitting of the data at high

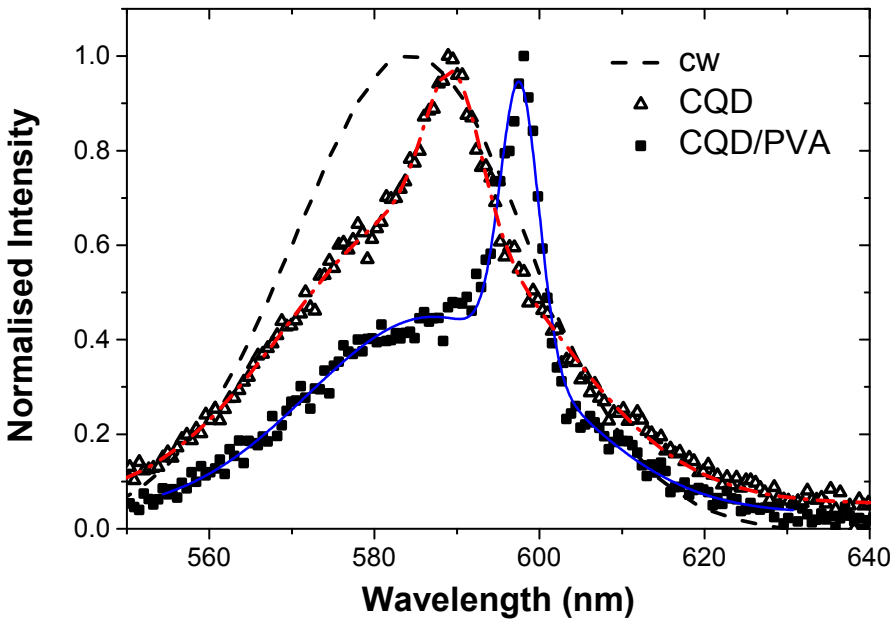

Fig. 3: cw edge PL (black dash line), CQD sample edge emission (data: open black triangles; fit: red dash-dot line) and CQD/PVA sample edge emission (data: black square; fit: blue solid line) under 5ns-pulse pumping.

fluence, where ASE dominates, using eq. (1) and only two fitting parameters, A and G. In these conditions, the relative comparison of G for the two samples gives an approximation for the gain enhancement brought by the addition of the PVA layer. It is found that this enhancement for G is 3 for a fluence F of 625 μJ/cm^2 (G=125 and G=40 for the CQD/PVA and CQD samples, respectively) corresponding to a relative increase in the modal gain g of 30%. This is of course advantageous for low threshold laser operation as is discussed in section 4.2.

Fig. 3 represents the normalized edge emission spectra of the CQD and CQD/PVA samples when pumped at 5 times the level above the onset of stimulated emission. The edge emission spectrum of the CQD sample under low intensity cw excitation is also plotted for information. Comparing the solution and film PL from Fig. 1(b) and Fig. 3 it can be seen that in the solid-state film a redshift of ~10nm is observed. This is due to the higher CQD density that leads to PL reabsorption. The contribution of non-radiative energy transfers, such as FRET [10], which exist in such a solid state, accounts for less than 2 nm of this shift. Compared to the cw edge PL at 584 nm characterised by a 35nm FWHM, the edge emission in the ASE regime is composed of a PL pedestal and a narrower ASE peak (see Fig. 3). The spectra can be decomposed into two Gaussians as is done in Fig. 3 for the CQD sample (red dash-dot curve) and the CQD/PVA sample (solid blue line). For the CQD sample, the PL pedestal is at 585 nm and the FWHM is slightly broader at 38 nm. The ASE peak is red-shifted by 4 nm at 589 nm compared to the PL pedestal while the FWHM is only 8 nm. Such a shift is attributed to a balance of gain and reabsorption in the film. The PL pedestal of the CQD/PVA sample is centred at 587 nm for a FWHM of 36 nm. The ASE peak is at 598 nm, i.e. red-shifted by 11 nm vs the edge PL, for a FWHM of 6 nm. The further red-shift is consistent with a quasi-3 level laser system: the higher modal confinement in the structure due to the PVA layer increases the modal gain, reducing the threshold with a net material gain peaking at longer wavelengths.

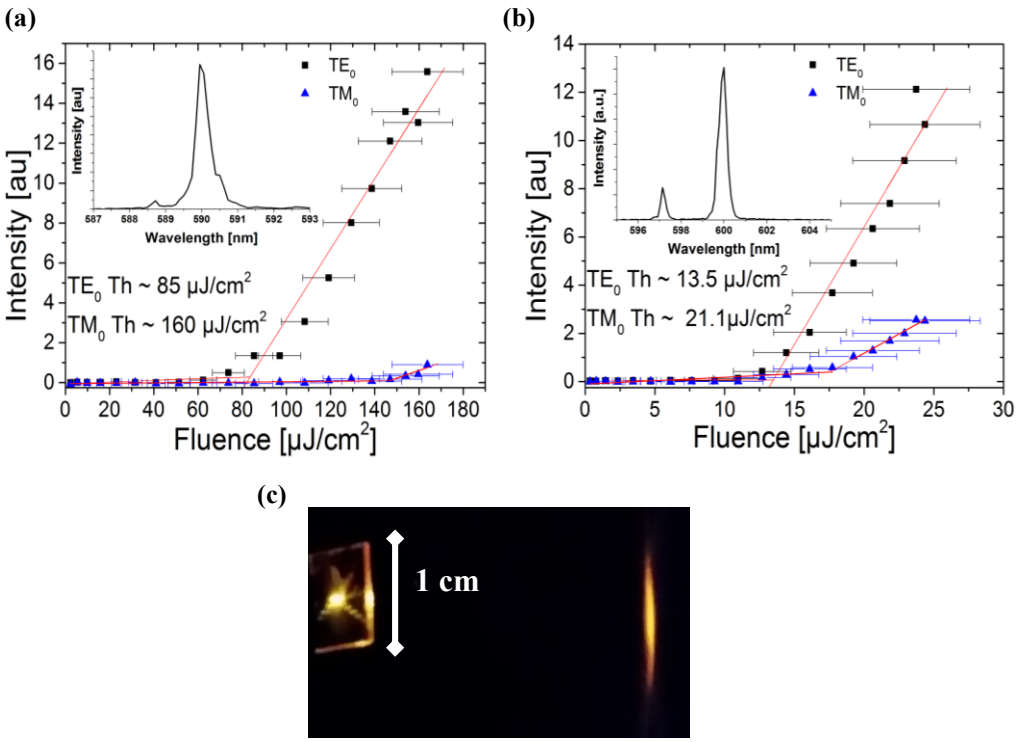

Fig. 4:Transfer function of a) CQD/DFB Neat laser, b) PVA/CQD.DFB laser with optical pump source, TM0 mode for corresponding samples. Inserts show emission spectra. c) PVA/CQD/DFB laser emission under optical pump.

These results demonstrate two things. The first is that the CdS_xSe_{1-x}/ZnS CQDs behave like a quasi-three level gain medium and that therefore the wavelength position of maximum optical gain can be tailored by design of the guide structure. The second is that despite this quasi-three level nature, low ASE threshold can be obtained. The bilyayer waveguide structure studied here reduces the ASE threshold to 380 μJ/cm^2 for a 300nm-thick CQD layer.

4.2 Laser characterisation

In this section, we characterise and compare the performance of DFB lasers made of a unique CQD layer and of the CQD/PVA bilayer. Fig. 4 shows the laser transfer function with the spectrum above laser threshold in inset. The laser with only a CQD layer, Fig. 4(a), emits TE-polarised light at 589.9nm with FWHM linewidth of 0.43 nm and has a threshold fluence of 85 ± 8.5 μJ/cm^2 – this is a significant threshold improvement over previously reported CQD lasers in the nanosecond regime having threshold fluence in the range of 500 to 4000 μJ/cm^2 [5, 22]). There is a secondary peak visible at 588.5 nm, which corresponds to the onset of the TM_0 mode, with an oscillation threshold at approximately 160 μJ/cm^2.The CQD/PVA DFB laser emits principally in the TE_0 mode at 600 nm but the TM_0 mode can be seen at 597 nm at high pump level, inset of Fig. 4(b). The 10nm shift of the oscillation wavelength compared to the CQD laser is due to an increase of the effective refractive index (1.55 for CQD vs 1.58 for CQD/PVA) of the mode caused by the presence of the PVA layer. The TE_0 total linewidth is 0.45 nm. The limitation in the linewidths for both CQD and CQD/PVA laser is attributed to the presence of lateral modes. The threshold fluence of the PVA/CQD DFB laser is only 13.5 ± 2.5 μJ/cm^2 (with the TM_0 threshold occurring at approximately 18 μJ/cm^2); an improvement of a factor of 6 when compared to the CQD laser.

This performance improvement is again partly due to the presence of the PVA layer which leads to a higher modal gain as discussed in section 4.1. However the x6 times reduction in threshold for the CQD/PVA laser is probably not entirely due to this gain enhancement. The modal overlap with the grating region of the sample without PVA is around 40% higher than for the CQD/PVA laser; this increases the mode interaction at the substrate and CQD layer interface, which might lead to higher scattering modal losses [36]. It has also been found that this was the case in organic laser based on 2nd-order DFB cavity for shallow grating and thin film, similar to our experimental conditions [36]. To our knowledge, this is the lowest threshold fluence reported for a CQD laser pumped with ns pulses. A 40nJ output pulse energy was measured with a photodiode for a pump fluence of 2.67 μJ, corresponding to a total efficiency, i.e. considering both top and bottom laser emission, of 3%.

5. Conclusion

We reported a yellow-orange CQD laser emitting with sub 10kW/cm^2 when pumped with 5ns pulses (13.5 ± 2.5 μJ/cm^2 threshold) . This performance is enabled by the use of alloyed-core/shell CdS_xSe_{1-x}/ZnS CQDs implemented in a bilayer DFB cavity, with the CQD gain film over-coated by a PVA layer. Study of the PL and ASE characteristics of the structure demonstrated that these CQDs behave like a quasi-3 level system. The bilayer structure is shown to increase the modal gain and we demonstrated ultra-low threshold for the onset of ASE, the lowest reported for nanosecond pumping regime. The performance reported here could lead to laser diode pumping of CQD lasers. This is appealing to take the technology out of the laboratory for applications such as bio-sensing [5].

Acknowledgment

This work was funded by EPSRC under projects:

EP/J021962/1 “Hybrid Colloidal Quantum Dot Lasers for Conformable Photonics”

EP/I029141/1 “Gallium Nitride Enabled Hybrid and Flexible Photonics”